

R. Pecnik, W.Sanz, A.Gehrer, J.Woiseschläger (2003) *Computation of laminar-turbulent transition in turbomachinery using an intermittency transport model*, - Proceedings 5th European Conference on Turbomachinery, Prague, 2003, pp 925-936

COMPUTATION OF LAMINAR-TURBULENT TRANSITION IN TURBOMACHINERY USING AN INTERMITTENCY TRANSPORT MODEL

Rene Pecnik, Wolfgang Sanz, Arno Gehrler and Jakob Woisetschläger

Institute for Thermal Turbomachinery and Machine Dynamics

Graz University of Technology

Graz, Austria

wolfgang.sanz@tugraz.at

ABSTRACT

The accurate numerical simulation of the flow through turbomachinery depends on the correct prediction of boundary layer transition phenomena. Heat transfer and skin friction investigations especially demand a reliable simulation of the transition process. Therefore, in this work a one-equation transport model for the turbulence weighting factor, which describes the intermittent laminar-turbulent flow, is implemented into a Navier-Stokes solver to simulate transition. The model was originally developed by Steelant and Dick [1] for the use in a conditionally averaged Navier-Stokes solver, and is now adapted for a Reynolds-averaged Navier-Stokes solver. In comparison to one-dimensional transition models, this new approach models the transition process not only in flow direction but also across the boundary layer.

The method is validated on transitional skin friction experiments on a flat plate (T3A test cases) and on heat transfer measurements in a linear turbine cascade done at the VKI. The results show good agreement with the experimental data and prove the usefulness of this new model for transition prediction.

INTRODUCTION

In turbomachines and especially in aircraft engines the Reynolds numbers that determine the evolution of the boundary layers are relatively low. So a large part of the flow along the blade surfaces is often laminar or transitional. The boundary layer development, losses, efficiency and heat transfer are greatly affected by laminar-to-turbulent transition. Due to the high turbulence levels by-pass transition is the dominant form of transition in turbomachinery.

The ability to accurately predict the transition process is crucial for the design of efficient and reliable machines. Considerable effort has been spent in investigating the ability of different turbulence models to predict transition for various flows. Besides these "pure" turbulence models, an increasing number of transition models are being developed from empirical correlations. They are used to modify the turbulence models to better predict the transition process. Most transition models are derived from boundary layer measurements on a flat plate and transition is described by an intermittency γ which gives the fraction of time when the flow is turbulent. In general, the models contain a criterion for the onset of transition on the blade and a formula for the determination of the intermittency in the transition zone in streamwise direction. In direction normal to the blade the intermittency is set to the value on the blade surface. This procedure neglects normal-to-the wall variations of the intermittency and the existence of free-stream turbulence in the pre-transitional region.

Intermittency transport models which describe a two-dimensional intermittency distribution can offer an improvement. Therefore in this work a one-equation transport model for a transitional weighting factor is presented. The model was originally developed by Steelant and Dick [1]. The model is discussed in detail to inform about the theoretical background and

to describe the modifications which were necessary for the implementation into a Reynolds averaged Navier-Stokes solver. The model is validated against skin friction and heat transfer measurement data to test its ability for accurate transition simulation.

NUMERICAL METHOD

Flow Solver:

The flow solver used in this investigation was developed by Gehrler [2] and is a full Navier-Stokes code. Time iteration of the mean-flow and turbulence equations is done by an implicit scheme based on a Newton procedure and applying local time stepping. The Euler fluxes are discretized using a third-order TVD-upwind, cell-centered scheme based on Roe's approximate Riemann solver. The viscous fluxes are evaluated by central differencing.

Turbulence Modeling:

The eddy viscosity is modeled by the Menter shear stress transport (SST) $k-\omega$ model [3]. It is a two-zonal model where the turbulence in the main flow is calculated by the $k-\varepsilon$ turbulence model, in the near-wall zone by the $k-\omega$ model. A blending function is applied to switch between both models. It produces almost fully turbulent flow in the boundary layer at the leading edge and is used as a baseline model to determine the eddy viscosity μ_t and other turbulent quantities in the computations.

TRANSITION MODELING

Transition is included by modifying the turbulent viscosity obtained by the turbulence model described above according to following equation:

$$\mu_t^* = f \cdot \mu_t \quad (1)$$

In general the factor f is the intermittency and is determined from analytical correlations as a streamwise function along the blade profile and is set constant in the direction normal to the wall. In this investigation the factor f is modeled with the help of a additional transport equation for a transitional weighting factor as proposed by Steelant and Dick [1]. In the following the transition model is described in detail.

Transition Model of Steelant and Dick (SD)

In 2001 Steelant and Dick presented a transition model, which is a derivative of the model they had proposed in 1996 [4]. The new model takes two effects into account, first the diffusion of the free-stream turbulent eddies into the boundary layer and second the transport and growth of the turbulent spots during transition.

Therefore a new turbulent weighting factor τ was proposed, which is the sum of the factors γ and ω :

$$\tau(x,y) = \gamma(x,y) + \omega(x,y) \quad (2)$$

- γ , the intermittency factor, describes the boundary layer transition.
- ω , the free-stream factor, describes the intermittency behaviour in the cross-stream direction prior to transition, with zero at the wall and continuously increasing to 1 in the free-stream.

A general transport equation for the factor τ contains convection, diffusion, spot production and dissipation terms and thus can be written as:

$$\frac{\partial \rho \tau}{\partial t} + \frac{\partial \rho u \tau}{\partial x} + \frac{\partial \rho v \tau}{\partial y} - D_\tau = P_\tau - E_\tau \quad (3)$$

Diffusion term: The general form is represented by the following equation containing a diffusion coefficient μ_τ , which is proportional to the molecular viscosity.

$$D_\tau = \frac{\partial}{\partial x_i} \left[(\mu_\tau) \frac{\partial \tau}{\partial x_i} \right] \quad (4)$$

To find a formulation for the diffusion coefficient Steelant and Dick postulated that the normal distribution of the free-stream factor ω prior transition corresponds to the inverse Klebanoff function, which is given with δ as the boundary layer thickness by:

$$\omega = \left(1 + 5(y/\delta)^6 \right)^{-1} \quad (5)$$

Some transformations lead to the following equation for the diffusion coefficient with $Tu_{le,\infty}$ as free-stream turbulence level at the leading edge and μ as molecular viscosity (for details see [1]):

$$\mu_\tau = 33 f_{\mu_\tau} \mu Tu_{le,\infty}^{-0.69} [-\ln(1-\tau)]^{-5(1-\tau)/6} \quad (6)$$

The constant 33 and the exponent $-5(1-\tau)/6$ were found by Steelant and Dick by several numerical experiments to obtain the best fitting with the inverse Klebanoff function. Because Steelant and Dick used conditioned averaged Navier-Stokes equations, the constant as well as the exponent had to be modified for these calculations (see below). The near wall function f_{μ_τ} ensures that close to a solid wall the diffusion ends up with zero.

Production term: The production term is defined by following equation with the density ρ and the velocity c and is set to zero upstream of the transition onset:

$$P_\tau = 2f_\tau (1-\tau) \sqrt{-\ln(1-\tau)} \beta \rho c \quad (7)$$

Concentrated breakdown is given by the linear law of the function $\sqrt{-\ln(1-\tau)}$. For distributed breakdown Steelant and Dick introduced the damping function f_τ :

$$f_\tau = 1 - e^{-1.735 \tan(5.45\tau - 0.95375) - 2.2} \quad (8)$$

The determining function of the production term is the spot growth parameter β (Eq. (9)). To consider compressibility and shock wave effects for the spot production rate $\hat{n}\sigma$, Steelant and Dick suggested the following modification to the incompressible spot production rate $\hat{n}\sigma_{inc}$, which results in an increased transition length with increasing Mach number.

$$\beta = \sqrt{\hat{n}\sigma_M (\lambda, Tu)} \frac{c\rho}{\mu}, \quad \hat{n}\sigma_M = \hat{n}\sigma_{inc} \left(1 + 0.58 M_{is}^{0.6} \right)^{-2} \quad (9), (10)$$

The incompressible spot production rate is usually set to the value for zero pressure gradient flows $\hat{n}\sigma_{ZPG}$. Steelant and Dick observed that the pressure gradient has a small effect on the spot growth during the initial phase of the transitional zone and introduced an additional function (12) into Eq. (11):

$$\hat{n}\sigma_{inc} = f_K \hat{n}\sigma_{ZPG}, \quad f_K = 1 + f_\tau (PRC - 1) \quad (11), (12)$$

with the pressure correction parameter PRC and the acceleration parameter λ_M defined as:

$$PRC = \begin{cases} \left(474 Tu_{le,\infty}^{-2.9}\right)^{1-e^{2 \times 10^6 \lambda_M}}, & \lambda_M < 0 \\ 10^{-3327 \lambda_M^{0.5985}}, & \lambda_M > 0 \end{cases}, \quad \lambda_M = -\frac{\mu_\infty}{\rho_\infty^2 U_\infty^3} \left| 1 - M_{is}^2 \right| \frac{dp}{dx} \quad (13), (14)$$

Finally, the spot production rate for zero pressure gradient flows $\hat{n}\sigma_{ZPG}$ is determined according to Mayle [5], with the local free-stream turbulence intensity Tu_∞ calculated from the value at the leading edge:

$$\hat{n}\sigma_{ZPG} = 1.25 \times 10^{-11} Tu_\infty^{7/4}, \quad Tu_\infty = Tu_{le,\infty} \left(\frac{U_{le,\infty}}{U_\infty} \right)^{3/2} \quad (15), (16)$$

Besides these modifications, Steelant and Dick noticed that a local strong adverse pressure gradient is still not sufficient to describe the sudden growth of the turbulent spots within a shock zone (see test cases MUR235 and MUR245 below). Therefore, in a first attempt to consider the shock wave influence Steelant and Dick modified the second parameter Tu_∞ in Eq. (16) based on the DNS results of Lee [6, 7] showing an increase in free-stream turbulence intensity by the factor of 5 or more in the presence of a shock wave. In this work the correction to Eq. (16) is not applied (see chapter "implementation" below).

Dissipation term: The dissipation term is constructed to guarantee a zero normal variation of the intermittency and thus of τ near the wall during the transition, a behaviour which is generally assumed. Based on the ideas of Cho and Chung [8] this can be achieved by a product of normal derivatives of velocity amplitude and τ in this source term. The factor μ_τ in following equation is the diffusion coefficient of Eq. (6). The constant C_3 was determined by Steelant and Dick to $C_3=2.5$ and also had to be adapted in this work.

$$E_\tau = C_3 \mu_\tau \frac{c}{c_\infty^2} \frac{\partial c}{\partial n} \frac{\partial \tau}{\partial n} \quad (17)$$

Transition onset: Steelant and Dick suggested a correlation based on the momentum thickness Reynolds number at transition onset, which takes into account the distributed breakdown (see [1]). Furthermore, they considered compressible effects, so that an increasing Mach number results in a delay of the transition onset:

$$Re_{\theta_{st,M}} = \sqrt{1 + 0.38M^{0.6}} Re_{\theta_{st,inc}}, \quad Re_{\theta_{st,inc}} = 0.664 \sqrt{400094 Tu_{le,\infty}^{-1.38} - 105254_{le,\infty}^{-7/8}} \quad (18), (19)$$

Boundary conditions: The wall boundary condition for the turbulence weighting factor τ is zero upstream of the transition onset location. Downstream of that position $\partial\tau/\partial y=0$ is applied. At the inlet $\tau=1$, thus allowing to impose an inlet turbulence level.

IMPLEMENTATION

In general the intermittency concept can be incorporated into the computations either by using conditioned averaged Navier-Stokes equations (e.g. Steelant and Dick [4]; Libby [9]) or by using the Reynolds averaged Navier-Stokes (RANS) equations and directly modifying the eddy viscosity obtained from a turbulence model. The first method leads to two sets of laminar and turbulent equations for mass, momentum and energy which are highly coupled by source terms, which depend on the turbulence weighting factor τ and model transition. For the latter method Simon and Stephens [10] showed that by combining the set of laminar and turbulent equations and by neglecting the Reynolds stresses in non-turbulent regions, the intermittency effect can also be considered with a modified eddy viscosity $\mu_t^*=\tau\cdot\mu_t$. Furthermore the conditioned averaged Navier-Stokes equations differ from the RANS equations by the presence of source terms, which depends on the turbulence weighting factor τ . This different implementation of transition into the main equations lead to different results for these concepts for the same transition model. Because in this work the SD turbulence weighting factor model is incorporated into a globally averaged (Reynolds averaged) Navier-Stokes solver, some modifications had to be made.

Modification of the parameters of the Steelant and Dick transition model

Diffusion term: The diffusion coefficient μ_t in Eq. (4) is responsible for the normal variation of τ prior to transition from zero at the wall to one in the free-stream (see Fig. 2) . Numerical experiments have shown that the initial constants 33 and 5/6 in the exponent of Eq. (6) are too large leading to a too slow increase of the turbulence weighting factor τ prior the transition, so that τ reaches a value of one not until $y/\delta=7$. Therefore the constant 33 was decreased by nearly a factor of 10 to obtain the best fitting with the inverse Klebanoff function according to Steelant and Dick. Finally the constants for the diffusion term in conjunction with the RANS equations had to be adjusted to (compare with Eq. (6)):

$$\mu_\tau = 3.5 f_{\mu_\tau} \mu Tu_{le,\infty}^{-0.69} [-\ln(1-\tau)]^{-0.25(1-\tau)} \quad (20)$$

Dissipation term: Another constant decisive for the distribution of the free-stream factor ω in cross-stream direction prior to the transition is C_3 in Eq. (17). To approach the inverse Klebanoff function C_3 for the sink term was determined to be $C_3=15.0$ instead of 2.5. Despite this modifications the agreement with the inverse Klebanoff function cannot be achieved for all turbulence levels.

Production term: Steelant and Dick's modification of the acceleration parameter leads in transonic regions with $M\approx 1$ to a value close to zero and loses its influence on the turbulent spot growth. Therefore in this work the original definition of the acceleration parameter is applied. Furthermore, with this modification there is no need to set the local free-stream turbulence intensity within a shock zone to 15%, as suggested by Steelant and Dick.

$$\lambda = \frac{v_\infty}{U_\infty^2} \frac{dU_\infty}{dx} \quad (21)$$

Several numerical experiments done by the authors showed that the intermittency increases too rapidly after the transition onset, so that the predicted length of the region of distributed breakdown is too short. Therefore the damping function f_τ in the production term in Eq. (7) is modified to extend the region of distributed breakdown. The following modified function f_τ (compare with Eq. (8)) gives better results for the test cases presented.

$$f_\tau = 1 - e^{-1.4 \tan(4.823\tau - 0.72877) - 1.15085} \quad (22)$$

DESCRIPTION OF THE TEST CASES

In this investigation numerical results are compared with experimental data obtained from transitional flows over adiabatic flat plates with sharp leading edges (Savill [11]). These experiments were designed to test the ability of turbulence models to predict transitional flow under the effects of free-stream turbulence and zero and varying pressure gradient conditions. In this work the test cases T3A and T3B are presented for zero pressure gradient flows. The flow region is modeled with H-type grids, the first grid point has a y^+ -value below 0.3. Table 1 gives velocity, turbulence level and the resulting turbulent viscosity at the inlet:

Table 1: Data of the flat plate test cases

	U_i [m/s]	Tu_{le} [%]	$(\mu_t/\mu)_i$ [-]
T3A	5.0	3.35	7.6
T3B	9.0	6.0	60.0

The ability of the transition model to predict transitional flow in conjunction with the globally averaged Navier-Stokes equations was also validated for the flow through a highly loaded transonic turbine guide vane designed and measured at the von Karman Institute VKI [12]. The measured heat transfer coefficients are compared with the computational results.

The most important geometrical data of the blade are: chord =67.647 mm, pitch to chord ratio =0.85, throat to chord ratio =0.2207 and a stagger angle of 55° measured from the axial direction. The total inlet temperature is set at $T_{01}=420K$ and the wall temperature is considered to be nearly at a constant level of 300K. The turbulence intensity was measured 55mm upstream from the leading edge and is given in Table 2. Since the transition model requires the turbulence level at the leading edge the correlation of Roach [13] is used, as no dissipation rate was measured at the experiments.

Table 2: Data of the MUR turbine test cases

	Tu_{le} [%]	$M_{2, is}$	$Re_{c,2}$
MUR235	4.52	0.927	1.15E6
MUR241	4.52	1.089	2.11E6
MUR245	3.36	0.924	2.13E6

RESULTS AND DISCUSSION

T3A and T3B test case

The computed skin friction distribution for the test cases T3A and T3B were compared with the experimental data and the analytic laminar and turbulent solution in Fig. 1 (top). For the T3A test case the model predicts transition onset at approximately $Re_x=40000$ using Eq. (18), (19).

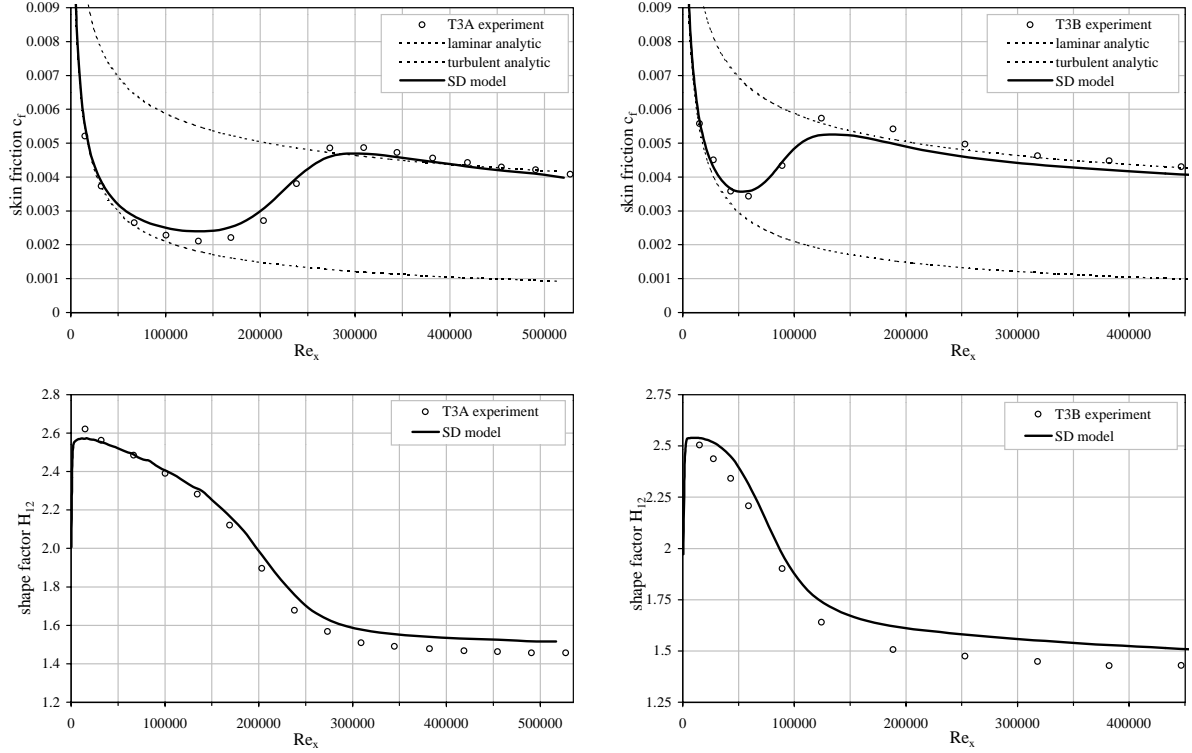


Fig. 1: Comparison of skin friction c_f (top) and shape factor H_{12} (bottom) for T3A (left) and T3B (right) test case

The numerical result calculated with the Menter SST turbulence model and the SD transition model matches the experimental data very well. Also for the test case T3B the computation agrees well with the measurement at the beginning of transition, but deviates slightly at end of transition, because the underlying Menter SST turbulence model provides to low turbulent quantities in the fully turbulent region.

The shape factor H_{12} , shown in Fig. 1 (bottom), is defined as the ratio of displacement thickness to momentum thickness in the boundary layer $H_{12} = \delta_1 / \delta_2$ and is influenced by the free-stream turbulent eddies prior to transition. In contrast to most existing transition models the SD model is able to consider the diffusion of the turbulent eddies into the underlying laminar boundary layer, changing the Blasius velocity profile, so that the measured decrease of the shape factor starting at the leading edge is well predicted for test case T3A. In test case T3B the agreement is also good, although the values are slightly higher than the measured ones.

One of the major features of the model is its ability to reproduce cross-stream intermittency profiles. Fig. 2 shows the normal-to-wall variation of the predicted turbulence weighting factor τ for several streamwise locations. Close to the wall the model predicts an increase of the factor τ from zero prior to transition to one at the end of transition ($Re_x > 400\,000$). Prior to the transition onset the quantity τ reduces to the free-stream factor ω (see Eq. (2)) and hence corresponds to the inverse Klebanoff function with zero at the wall and a gradual increase to full free-stream turbulence with $\tau=1$ at $y/\delta=1.5$, so that it allows the consideration of the free-stream turbulence. Downstream of the predicted transition onset ($Re_x=130\,000$) the intermittency factor γ simulates the growth of the turbulent spots and therefore close to the wall τ increases to $\tau=1$ till to the end of transition. At the outer region of the boundary layer the fully turbulent condition moves from $y/\delta=1.5$ to $y/\delta=0.5$.

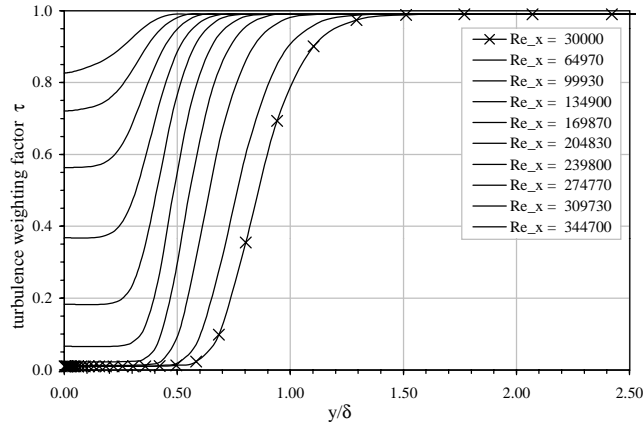


Fig. 2: Normal-to-wall variation of the turbulence weighting factor τ for the T3A test case

Transonic turbine guide vane (MUR test case)

Fig. 3 shows the blade contour of the MUR turbine guide vane designed by VKI. The computational grid is a multi-block grid with two H-type grids at the inlet and outlet region and an O-grid wrapping around the blade (192 x 65 grid points). The maximum value of y^+ is about 0.2. The Mach number contours are shown for the test case MUR241 with an exit Mach number of 1.089. There is a suction side shock wave starting close to the trailing edge which cuts the wake. The maximum Mach number occurs on the suction side close to mid chord.

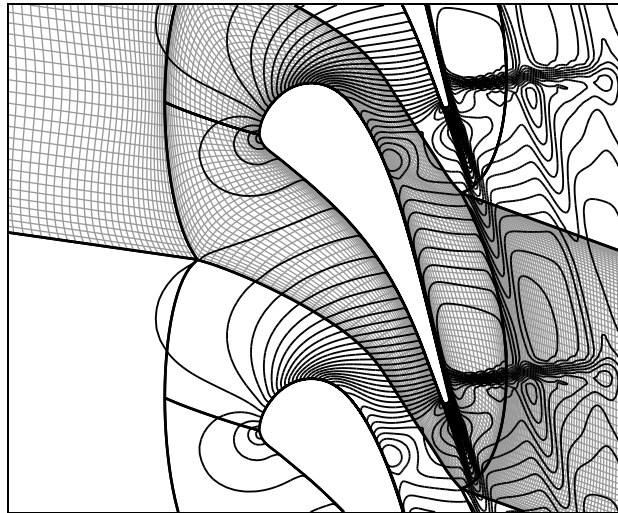


Fig. 3: Mach number contours for the MUR241 test case and block boundaries of the computational grid

The calculated isentropic Mach number distributions for all test cases are given in Fig. 4 together with the only available experimental data at slightly different Mach numbers. The test cases MUR235 and MUR245 only differ in the Reynolds number, so that the Mach number distribution is nearly the same. The MUR241 case shows a far more downstream shock position compared to the experiment at a smaller exit Mach number. For the MUR test cases the heat transfer distribution is compared between experiment and computation, because this quantity is very sensitive to the correct prediction of the boundary layer behaviour. At first, the influence of the turbulent mixing length at the inlet boundary and of the turbulence production term are discussed by the heat transfer distribution for the MUR235 test case without any transition modeling (Fig. 5). If the Menter SST $k-\omega$ model is used with the original production term, which only depends on the strain rate, and if $l_m/c=0.05$ is chosen as inlet bound-

any condition for ω , the heat transfer is significantly overpredicted. One reason is that this production term leads in regions with high normal strains as close to the leading edge stagnation point to large unphysical production of turbulent kinetic energy. By decreasing the inlet turbulent mixing length to $l_m/c=0.005$, which corresponds to an increase of the specific turbulent dissipation rate at the inlet, the calculated heat transfer reduces considerably, but is still higher than the experimental data. A further decrease can be achieved by modifying the turbulent production term to be a function of the vorticity $P_k=\mu_t\Omega^2$, which avoids the aforementioned leading edge problems. In this case the heat transfer is predicted too low on the suction side close to the leading edge, but it is interesting that now the dependency on the inlet condition is very small. Although the modified production term avoids the unphysical turbulence production, the combination of modified turbulence model and SD transition model results in even lower heat transfer coefficients. Therefore, for all test cases the Menter SST turbulence model was used with the standard production term and for the MUR235 test case with $l_m/c=0.005$ at the inlet boundary.

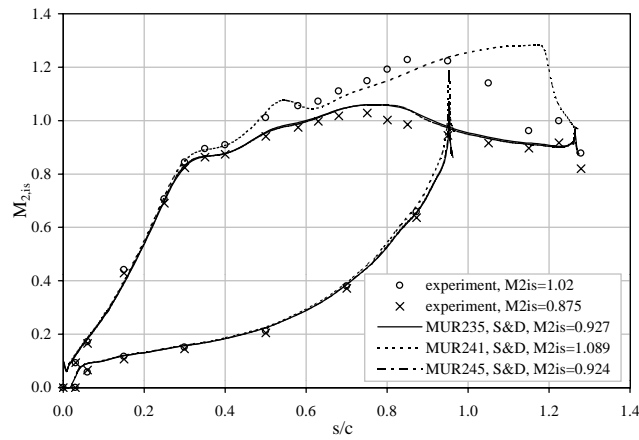


Fig. 4: Comparison of the calculated isentropic Mach number distributions for the MUR235, MUR241 and MUR245 test cases with experiments, Menter SST turbulence model in conjunction with the SD model

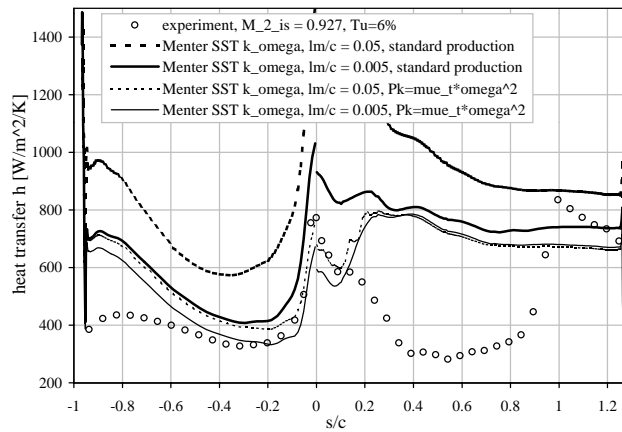


Fig. 5: Heat transfer distribution for the MUR235 test case: comparison of fully turbulent solutions with different production terms and inlet boundary conditions for ω

The heat transfer distribution for the applied transition model compared with the fully turbulent solution and the experimental data is given in Fig. 6 for the test case MUR235 (4.52% inlet turbulence intensity). Although the diffusion process of the turbulent eddies towards the laminar boundary is considered by the SD model, the heat transfer of the laminar boundary layer agrees well with the experimental data only on the suction side. The reason for

this difference between suction and pressure side is that the high turbulence close to the stagnation point produced by the (standard) original production term of the Menter SST turbulence model is transported only along the suction side. The observed sudden increase at $s/c=0.85$ is predicted well although the somewhat arbitrary setting of the local turbulence intensity Tu_∞ to 15% as done by Steelant and Dick [1] in the shock region was not applied, as mentioned before. But the level of the increased turbulent heat transfer downstream of $s/c=0.85$ is captured well again. The intermittency γ shows that on the suction side transition starts at $s/c=0.20$ and ends at the trailing edge with a value of 99%. On the pressure side transition onset is predicted at $s/c=0.55$ and remains transitional till to the trailing edge with $\gamma=30\%$, whereas the experimental data indicate a laminar boundary layer till the trailing edge.

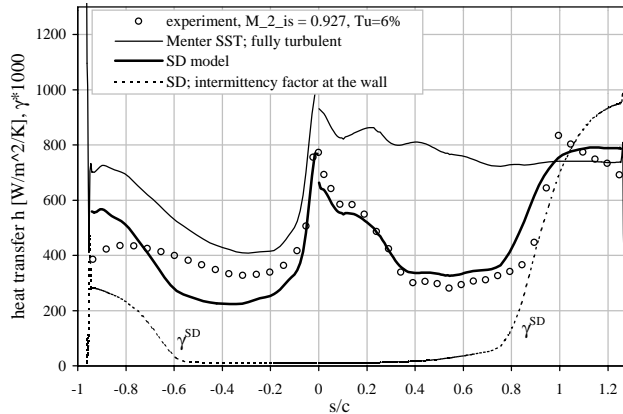


Fig. 6: Heat transfer distribution for the MUR235 test case

Fig. 7 shows the turbulent kinetic energy in the largely magnified inner boundary layer region up to $y^+=1000$, with the fully turbulent and the transitional solution. In both figures the turbulent kinetic energy displayed was limited to $600\text{m}^2/\text{s}^2$. The fully turbulent solution shows on the suction side an inner region ($y^+ > 10$) of high turbulence starting at the leading edge and extending till to the trailing edge. A second region confined from $s/c=0.15$ to $s/c=0.7$ is located more outside ($y^+ > 100$) and results from the turbulent production term based on the strain rate.

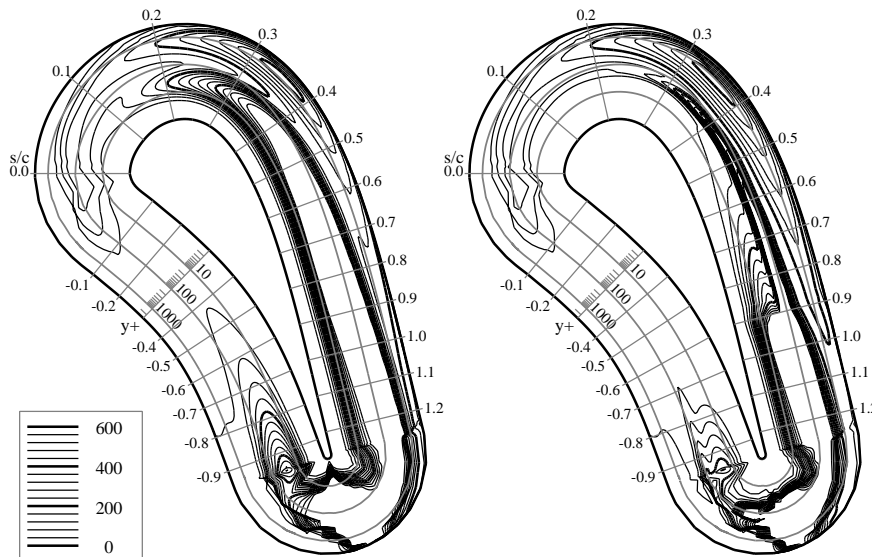


Fig. 7: Turbulent kinetic energy around the blade for the MUR235 test case (inner region till $y^+ = 1000$ largely magnified, k range $< 600\text{m}^2/\text{s}^2$): left = fully turbulent solution, right = SD transition model

On the pressure side, the boundary layer becomes turbulent at $s/c=-0.4$. The SD transition model suppresses the turbulence in the inner region ($y^+ < 30$) till to the transition onset location (about $s/c=0.3$). Then turbulence grows, although the boundary layer becomes highly turbulent not before $s/c=0.9$. The existence of turbulence at the outer region of the boundary layer is the reason for the better prediction of the influence of free-stream turbulence on the heat transfer in the region of the laminar boundary layer. On the pressure side the transition takes place more downstream than in the fully turbulent solution.

The test case MUR241 differs from test case MUR235 in a higher outlet Mach number and a higher outlet Reynolds number. Therefore the experimental heat transfer coefficient (Fig. 8, left) at the leading edge is about $200\text{W/m}^2\text{K}$ higher than in the MUR235 test case. Even though the Mach number distribution on the pressure side for all test cases is nearly the same the heat transfer distribution differs compared to MUR235 test case. The SD transition model computes an earlier transition onset on the pressure side at $s/c=-0.3$. Between $s/c=0$ and $s/c=-0.3$ the predicted heat transfer is too low, as in test case MUR235. Close to the trailing edge, where transition is close to 60 %, the heat transfer is of the same size as in the measurement. On the suction side the overall calculated heat transfer agrees well with the experimental data. The rise in intermittency at $s/c=0.55$ can be explained by the decelerated flow downstream of the local Mach number maximum at the suction side (see Fig. 3 and Fig. 4). Near to the trailing edge a shock exists, which leads to a sharp increase in intermittency up to 80 % and thus in heat transfer.

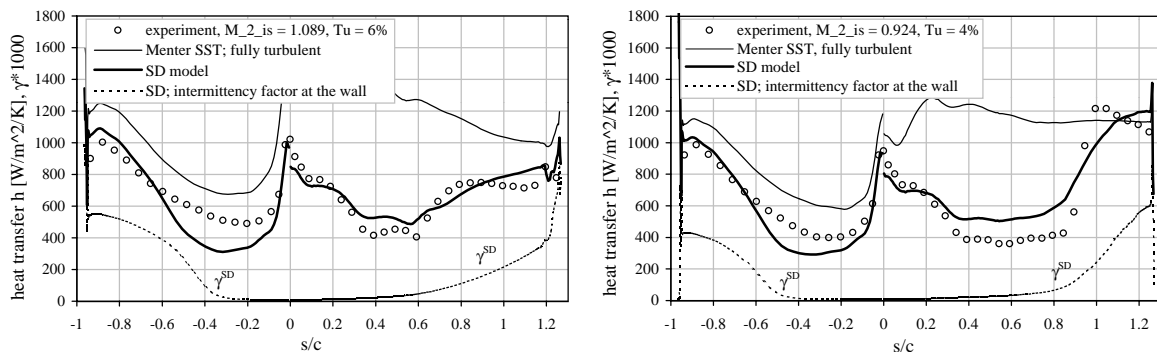


Fig. 8: Heat transfer distribution for the MUR241 (left) and the MUR245 (right) test case

The test case MUR245 in Fig. 8 (right) is similar to MUR235, but the exit flow Reynolds number of 2.1×10^6 is about twice as high and the inlet turbulence level is lower. The SD model predicts a too high heat transfer at the mid chord of the suction side. A possible explanation is that the dependency of the free-stream factor ω on the turbulence level is not correctly modeled. The sudden rise at $s/c=0.85$ is not predicted by the SD transition model, because the manual setting of the local turbulence level to 15% at the shock position was not applied (see also test case MUR235). On the pressure side from $s/c=-0.6$ till to the trailing edge the calculated heat transfer agrees with the experimental value. Before transition onset the heat transfer is again under-predicted.

CONCLUSION

Algebraic transition models which are used more frequently nowadays to consider laminar-to-turbulent transition in the flow design of turbomachinery blades suffer from the neglect of normal-to-wall variation of the transition process and of the existence of free-stream turbulence. Therefore in this work a one-equation transport model for a transitional weighting factor was investigated. The selected model by Steelant and Dick [1] model predicts normal-to-wall variation of transition, and this allows consideration of the influence of free-stream tur-

bulence on the laminar boundary layer.

The model was adapted and incorporated into a Reynolds-averaged Navier-Stokes flow solver. Several test cases were evaluated and the results show a remarkable improvement compared to fully turbulent solutions for most test cases. For highly turbulent flows the SD model gives good results for the prediction of the boundary layer shape factor, of density fluctuations as well as of the heat transfer in a laminar boundary layer due to the consideration of the free-stream turbulence. Although the SD model also shows some deficiencies it is a promising approach for future improved transition modeling.

ACKNOWLEDGMENTS

This work was partly supported by the Austrian Science Foundation (FWF) and the Austrian Ministry for Education, Science and Culture (BMBWK) within the grant Y57-TEC (Non-Intrusive Measurement of Turbulence in Turbomachinery).

REFERENCES

- [1] Steelant, J., Dick E. (2001), *Modeling of Laminar-Turbulent Transition for High Freestream Turbulence*, Journal of Fluids Engineering, Vol. 123.
- [2] Gehrler, A., (1998), *Entwicklung eines 3d-Navier-Stokes Code zur numerischen Berechnung der Turbomaschinenströmung*, PhD Thesis at Graz University of Technology
- [3] Menter, F.R., (1994), *Two-Equation Eddy-Viscosity Turbulence Models for Engineering Applications*, AIAA Journal, Vol. 32, No. 8, August, pp. 1598-1605.
- [4] Steelant, J., Dick, E., (1996), *Modelling of Bypass Transition with Conditioned Navier-Stokes Equations coupled to an Intermittency Equation*, International Journal for Numerical Methods in Fluids, Vol. 23, 193-220.
- [5] Mayle, R.E., (1991), *The Role of Laminar- Turbulent Transition in Gas Turbine Engines*, Journal of Turbomachinery, Vol. 113, pp. 509-537.
- [6] Lee, S., Lele, S.K. and Moi, P., (1993), *Isotropic Turbulence Interacting with a Weak Shock Wave*, Journal for Fluid Mechanics, 251, and corrigendum 264:373-374, 1994, pp. 533-562.
- [7] Lee, S., Lele, S.K. and Moi, P., (1997), *Interaction of Isotropic Turbulence with Shock Waves: Effect of Shock Strength*, Journal for Fluid Mechanics, 340, pp. 225-247.
- [8] Cho, R., Chung, M.K., (1992), *A $k-\epsilon-\gamma$ Equation Turbulence Model*, J. Fluids Mech., 237, pp. 301-322.
- [9] Libby, P. A., (1975), *On the prediction of intermittent turbulent flows*, J. Fluid Mech., 868, 273-295 (1975).
- [10] Simon, F.F. and Stephens, C.A., (1991), *Modeling of the Heat Transfer in Bypass Transitional Boundary-Layer Flows*, NASA Technical Paper 3170.
- [11] Savill, A M., (1992), *A synthesis of T3 Test Case Predictions*, Numerical Simulation of Unsteady Flows and Transition to Turbulence, O. P. et al., ed., Cambridge University Press, pp. 404-442.
- [12] Arts, T., Lambert de Rouvriot, M., Rutherford, A. W., (1990), *Aero-thermal Investigation of a Highly Loaded Transonic Linear Turbine Guide Vane Cascade*, Technical Note 174, von Karman Institute for Fluid Dynamics, Belgium.
- [13] Roach, P. E., (1987), *The generation of nearly isotropic turbulence by means of grids*. International Journal of Heat and Fluid Flow, pp.82-92.